

## Effect of Pattern Geometry on the Fracture Behavior of Direct Bonded Silicon Wafers

Hyun-Joon Kim-Lee<sup>a</sup> and Kevin T. Turner<sup>a, b</sup>

<sup>a</sup> Materials Science Program, University of Wisconsin, Madison, WI 53706, USA

<sup>b</sup> Dept. of Mechanical Engineering, University of Wisconsin, Madison, WI 53706, USA

The effect of shallow and deep etched interface patterns on the adhesion of silicon-silicon direct bonds is examined. Specifically, fracture loads of double cantilever beam specimens with structured interfaces, with dimensions in the micrometer regime, are measured. The results show that the interface fracture load increases as the structures, which are simple pillars, become taller and narrower. These experimental results are in good agreement with finite element modeling results. The fracture surfaces were inspected after testing, and the surfaces generally had very little debris from the bonded pillars. The results of this study may help to aid in the design of temporary bonding processes that use patterned interfaces to tune failure behavior.

### Introduction

Temporary wafer bonding is an important step in thin layer transfer processes for the fabrication of complex substrates and three-dimensional integrated circuits (3-D ICs). However, effective temporary bonding that provide good adhesion during transfer and easy and clean release has been a constant challenge (1). In the present work, we explore the tuning of interfacial adhesion of direct bonded interfaces using patterned and structured interfaces as a means to tailor adhesion in temporary bonding processes.

Patterning on bonded wafer interfaces can have a dramatic effect on the adhesion and fracture properties of the interfaces (e.g. (2, 3)). However, there remains a lack of understanding of precisely how patterning affects the mechanical properties of wafer-bonded interfaces. In this work, the effect of shallow and deep patterns at the interface of silicon direct bonded specimens is examined. The effects of a range of pillar-based pattern geometries (pillar height = 1.1 – 54.0  $\mu\text{m}$ , width = 5 – 30  $\mu\text{m}$ ) at the interface of double cantilever beam (DCB) are examined experimentally and through mechanics modeling. The purpose of the study is to understand the role of interface geometry in determining the fracture behavior of silicon-silicon direct bonds. The results may be helpful in tailoring the adhesion properties of wafer bonded interfaces for applications such as temporary bonding.

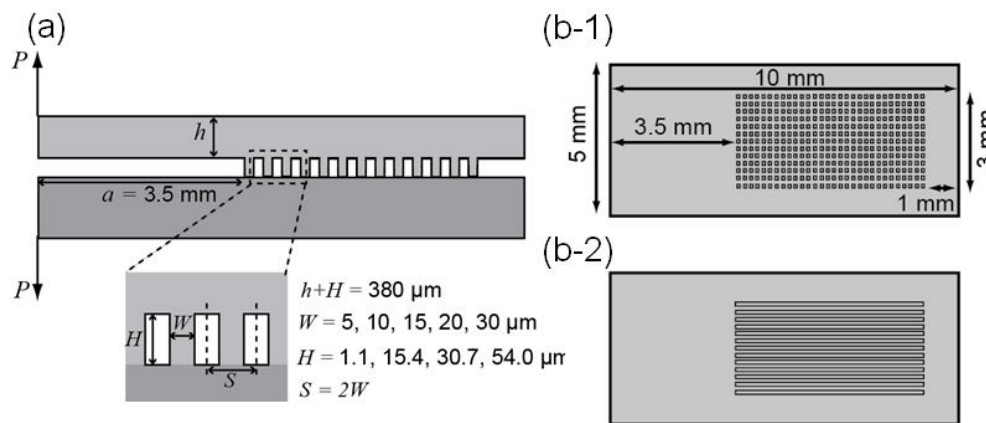


Figure 1. Geometry of the fabricated specimen. (a) sideview, (b-1) top view, (b-2) specimen with the line patterns used as a control “unpatterned” specimen. The specimen in (b-2) is used instead of a completely unpatterned interface as a control specimen to facilitate comparison to 2-D modeling results.

## Experimental Procedure

### Specimen Fabrication

Double cantilever beam fracture specimens with patterned interfaces, as described in Figure 1, were fabricated from 100 mm diameter Si (100) wafers. One set of wafers was processed to have pillar arrays with various lateral and vertical dimensions. Arrays of squares and rectangles with a range of dimensions (pillar width = spacing = 5, 10, 15, 20, and 30  $\mu\text{m}$ ) were patterned on the wafers using photolithography. Each wafer in the set was etched for different lengths of time using deep reactive ion etching, and the resultant pillar heights on the four wafers in this study were 1.1, 15.4, 30.7, and 54.0  $\mu\text{m}$ . This results in pillar patterns with a range of aspect ratios (height to width) as shown in Fig. 2.

The patterned wafers were bonded to unpatterned wafers to create the specimens. Prior to bonding, wafers were cleaned in a 25% HF solution followed by a piranha solution ( $\text{H}_2\text{SO}_4:\text{H}_2\text{O}_2 = 4:1$ ) and water rinse. The wafers were direct-bonded at room

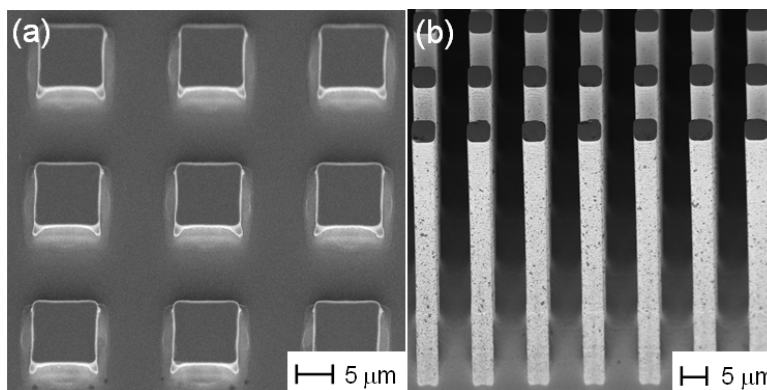


Figure 2. SEM micrographs of fabricated pillar structures: (a)  $H = 1.1 \mu\text{m}$ ,  $W = 10 \mu\text{m}$ , (b)  $H = 54.0 \mu\text{m}$ ,  $W = 5 \mu\text{m}$ .

temperature immediately after cleaning. The bonded pairs were inspected using infrared (IR) transmission imaging to confirm that the bonds were free of large voids. An example of an inspection image is shown in Figure 3. After room temperature bonding, wafer pairs were annealed at 425°C for 48 hours to enhance the bond toughness (4). After annealing, individual specimens (10mm × 5mm) were diced from the bonded wafers. Less than 5 % of the chips were lost due to failure during the dicing process. Specimens with identical patterns were located randomly across the wafer. Unpatterned DCB specimens and the specimens with line patterns (Fig. 1(b-2)), where the lines are continuous in the crack propagation direction, were also prepared in the same wafer pairs for the comparison. After dicing, the specimens were cleaned in acetone, methanol, and isopropanol and dried at 50°C for 24 hours.

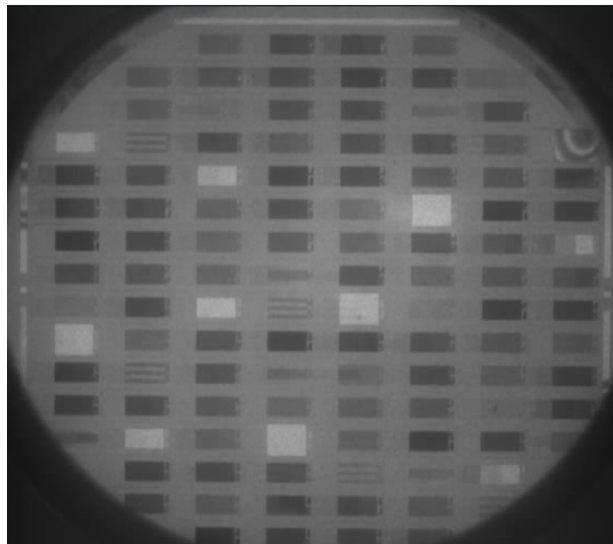


Figure 3. An example of IR inspection image of the bonded wafer pairs. The height of the pillars is 54  $\mu\text{m}$ . In this example, the overall bond quality is good except one specimen in upper right of the image where a fringe pattern is clearly visible.

### Fracture Test

The schematic of the fracture test setup used is shown in Figure 4(a). The studs that connect the specimen to the load frame are made of brass with 3 mm × 3 mm cross section and are glued to the top and bottom of the specimen. The lower clevis of the load frame was fixed at the bottom and the upper block was connected to a 20 N load cell which was displaced at a constant rate using a piezoelectric-based actuator. Load and displacement values were recorded as the load cell was translated with the actuator at a rate of 800 nm/sec. A typical load – displacement plot is shown in Figure 4(b). The maximum load in the test is defined as the fracture load ( $P_F$ ). The overall fracture behavior of the specimen can also be observed from the force displacement plot. After the tests, fracture surfaces were examined via optical and scanning electron microscopy to check if the fracture occurred at the interface.

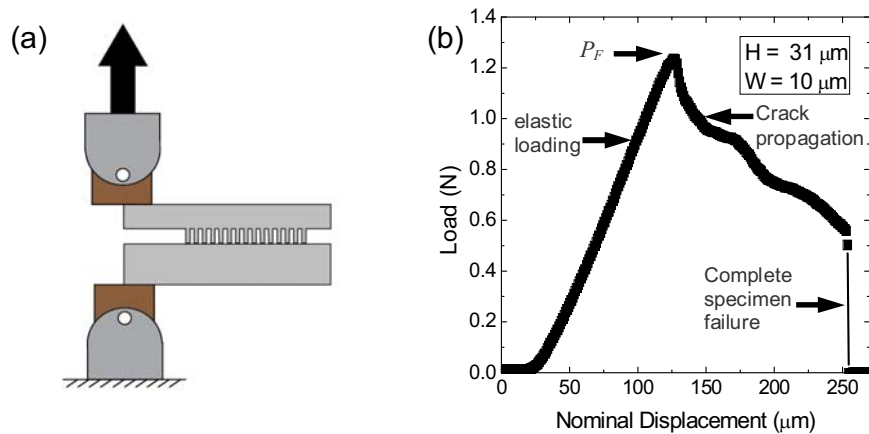


Figure 4. (a) Schematic of the fracture test setup, (b) a typical load – displacement plot showing the fracture load ( $P_F$ )

## Results and Discussion

### Measured Fracture Loads

The measured fracture loads are shown in Figure 5 and demonstrate a clear dependence of fracture behavior on pattern geometry. Fracture loads increase with pillar height for all pillar width values. The fracture loads also increase as the pillar becomes narrower except when the pillar height is 1.1  $\mu\text{m}$ . The fracture loads for  $H = 1.1 \mu\text{m}$  do not vary significantly with the pillar width and the values are similar to those of the “unpatterned” case. Note that the specimen with the highest aspect ratio pillars has a fracture load of  $2.5\times$  that of the control specimen even though the bonded area is reduced.

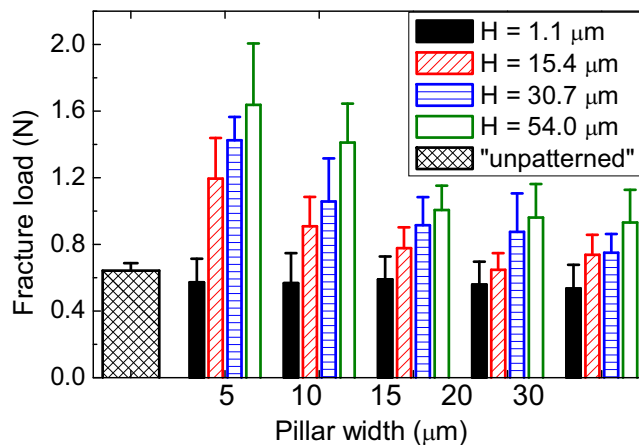


Figure 5. Results of the fracture load measurements. The fracture load values for the specimens with line patterns where lines are parallel to the crack propagation direction and the pattern height is 1.1  $\mu\text{m}$  are defined as the control “unpatterned” case.

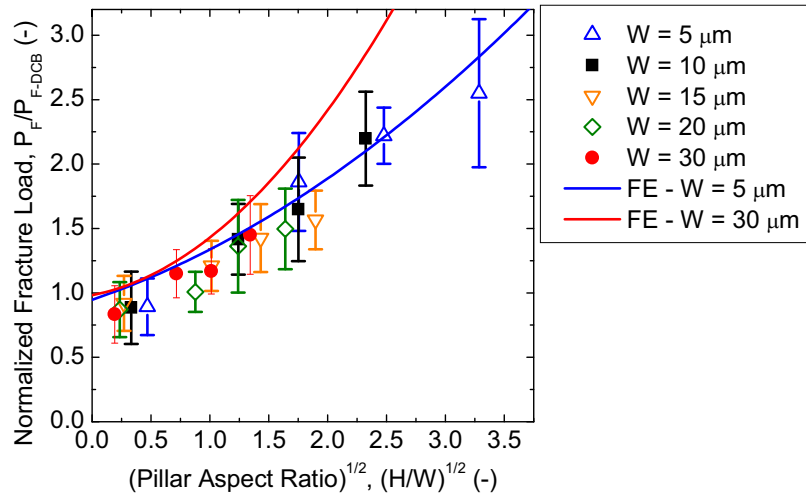


Figure 6. Normalized fracture load as a function of the square root of pillar aspect ratio obtained from experimental measurements. The experimental values are compared to the results from finite element simulations.

#### Modeling Results and Interpretation of Data

In order to interpret the experimental results, analytical and finite element (FE) mechanics models were developed to examine the failure of patterned silicon interfaces. A simplified 2D analytical model predicted the normalized fracture load ( $P_F/P_{F-DCB}$ ), where  $P_{F-DCB}$  is the fracture load for an unpatterned DCB specimen, would be proportional to the square root of  $(H/W)$  assuming that the spacing between pillars are same as the pillar width and there are defects near the edge of the pillar that can act pre-cracks. The analytical model shows that the fracture load increases with the aspect ratio of the pillar because the pillars increase the compliance of the interface, which leads to a more equal distribution of stress at the interface. Although the analytical models give the insight into the essential scaling of fracture load with pattern geometry, the simplified nature of the models prevents a quantitative prediction of the fracture load. Therefore, finite element modeling was used to obtain more precise prediction of the effect of interface patterning.

In the finite element modeling, a 2-D model of the whole DCB specimen with a patterned interface is constructed. It is assumed that there is a pre-crack at the edge of the first pillar interface with a length equal to 10% of the pillar width. The strain energy release rate for the specimen is calculated in the model using the virtual crack closure technique (5). The fracture load  $P_F$  is obtained with the calculated total strain energy release rate and the interface toughness. Fits to the results of the FE modeling are shown in Figure 6. The curves show a similar scaling with pillar aspect ratio for high aspect ratio pillars.  $P_F$  asymptotically approaches  $P_{F-DCB}$  as  $H/W$  goes to zero, since the specimen essentially becomes unpatterned as  $H/W$  goes to zero. The experimental results generally agree with the FE modeling results. This agreement suggests that the FE modeling can be used effectively to predict the fracture load of the patterned specimens.

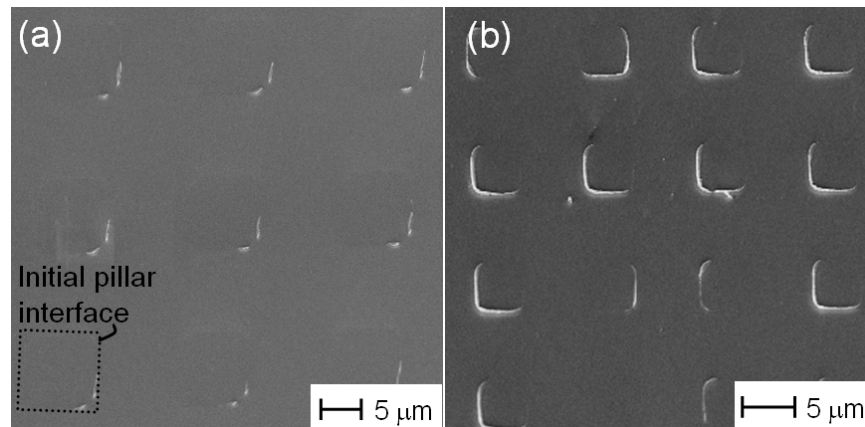


Figure 7. SEM micrographs of fracture surfaces of the specimens. These surfaces were flat and smooth prior to bonding. Original pillar geometries were (a)  $H = 1.1 \mu\text{m}$ ,  $W = 10 \mu\text{m}$ , (b)  $H = 54.0 \mu\text{m}$ ,  $W = 5 \mu\text{m}$ . Small parts of pillars fractured and remained on the surface after specimen failure. Still the crack propagates primarily at the interface. The crack propagated from left to right for both cases.

### Fracture Surfaces

SEM images in Figure. 7 show that the fractured surfaces of the specimens are not perfectly smooth. Pillars that are separated from the interface appear to leave a small part of the pillar behind on the unpatterned surfaces. Obviously, a cleaner fracture surface would be required if structured interfaces were to be used in temporary bonding processes. Tuning of the annealing and loading conditions for cleaner fracture surfaces is currently being investigated.

### **Conclusions**

In conclusion, we have examined the role of patterning in the fracture behavior of direct bonded silicon interfaces using patterned DCB specimens. The fracture load measurements showed that the high aspect ratio pillar patterns require larger fracture load for the failure and the fracture load for patterned specimens are larger than that of the control specimens with greater bonded area. This experimentally observed trend agrees with results from finite element simulations. The trend is explained by the fact that taller pillars lead to lower interface stiffness and, hence, a more even load distribution at the interface. Observation of the failed surfaces suggests that this direct-bond and annealing process and patterned DCB specimens must be used with caution if clean fracture surfaces for temporary bonding applications are desired. The data and models provided here can be used to design interfaces with specific interfacial response for temporary bonding processes.

### Acknowledgments

This work was supported by NSF funded Materials Research Science and Engineering Center at the University of Wisconsin - Madison (NSF Award # 0520527), AFOSR-MURI FA9550-08-1-0337, and a student research grant from the semiconductor wafer bonding symposium of the 214th ECS meeting.

### References

1. Puligadda et al., *Mater. Res. Soc. Symp. Proc.* **970**, 0970-Y04-09 (2007)
2. Tadepalli et al., *Acta Mater.* **56**, 438 (2008).
3. Landis et al., *Nanotech.* **19**, 125305 (2008).
4. Q.-Y. Tong and U. Gösele, *Semiconductor Wafer Bonding: Science and Technology*, p. 118, Wiley Interscience, New York (1999).
5. R. Krueger, *Appl. Mech. Rev.*, **57**, 109 (2004).